Soft Matter

Dynamic Article Links

Cite this: *Soft Matter*, 2012, **8**, 6693

www.rsc.org/softmatter

PAPER

Model, self-assembly structures, and phase diagram of soft Janus particles†

Zhan-Wei Li,[a] Zhong-Yuan Lu,[b] Zhao-Yan Sun*[a] and Li-Jia An[a]

Received 21st February 2012, Accepted 1st May 2012
DOI: 10.1039/c2sm25397f

Janus particles exhibit interesting self-assembly behavior and functional performances. In particular, soft and deformable Janus particles, as diverse as Janus micelles, Janus microgels, and Janus dendrimers, should receive more attention due to their unique chemical and physical properties and enormous potential applications. Gaining control over precise and predictable self-assembled structures and understanding the fundamental details of self-assembly remain a formidable challenge. Here we present a novel mesoscale model for soft Janus particles, which successfully reflects their physical nature by directly mapping onto experimentally measurable particle properties. By properly tuning Janus balance and the strength of attraction between attractive patches, soft Janus particles can reversibly self-assemble into a number of fascinating hierarchical superstructures in dilute solutions, such as micelles, wormlike strings, single helices, double helices, bilayers, tetragonal bilayers, and complex supermicelles. Our work demonstrates that soft Janus particles with deformable and non-centrosymmetric characteristics hide many surprises in the design and fabrication of hierarchically self-assembled superstructures.

1 Introduction

An almost unbelievable revolution in materials science has been enabled by anisotropic particles.[1,2] Janus particles have received significant attention due to the unique feature of being non-centrosymmetric and the possibility of generating fascinating hierarchical superstructures with diverse promising applications such as drug delivery, optical and electronic sensors, and interface stabilizers.[3–9] Both the design and fabrication of new Janus particles will be sure to bring more exciting hierarchical superstructures.

Janus particles may be classified into two categories: rigid Janus particles and soft Janus particles. So far there have been a number of studies in experiments,[10,11] theory,[12] and computer simulations[13–17] regarding the self-assembly of rigid Janus particles, by which a large variety of hierarchically self-assembled structures have been observed. For example, it has been proved that highly ordered fibrillar triple helices and even Kagome lattices can be realized using rigid Janus particles or triblock Janus particles.[18–21]

Unlike typical rigid Janus particles, soft Janus particles are able to deform and overlap. They include Janus micelles,[4,5,22,23] Janus microgels,[24] and Janus dendrimers,[25–28] which can be prepared by the self-assembly of block copolymers, atom transfer radical polymerization, and divergent or convergent approaches. The modulus of soft Janus particles may be controlled by varying the cross-linking density,[23,29] the grafting density,[24] the number of primary branches and the density of radial branches,[25] and so on. Due to their soft and deformable nature,[29] soft Janus particles may generate strikingly new self-assembled superstructures that cannot be obtained with conventional rigid colloidal particles.[22,23,25–27]

Since the modulus of soft Janus particles can be readily modified by changing the ambient conditions, their physical nature falls between near-hard-sphere colloids and ultra-soft colloidal systems.[30] Because of their complexity, it is a challenging task to gain insight into the fundamental details and processes of the self-assembly of soft Janus particles. Coarse-grained molecular dynamics by fitting all-atom simulations of the Janus dendrimer bilayers has provided a scheme for simulating the self-assembly of Janus dendrimers.[25,31] In fact, the diameters of soft Janus particles typically are in the range 10–1000 nm,[22,23,25–27,30] and the length scales of their self-assembly structures will be much larger, thus a mesoscopic coarse-grained description of a soft Janus particle as a whole from its physical nature may be a more feasible and efficient scheme to study the self-assembly of soft Janus particles over greater length and time scales.

Here, we introduce a novel mesoscale model specifically designed to study the self-assembly of soft Janus particles. The surface of a soft Janus particle is simply divided into repulsive

[a]*State Key Laboratory of Polymer Physics and Chemistry, Changchun Institute of Applied Chemistry, Chinese Academy of Sciences, Changchun 130022, China. E-mail: zysun@ciac.jl.cn*
[b]*Institute of Theoretical Chemistry, State Key Laboratory of Theoretical and Computational Chemistry, Jilin University, Changchun 130023, China*

† Electronic supplementary information (ESI) available: The relation between α_{f1}^{4} and G or δ; typical self-assembled structures for larger system sizes; the effect of ϕ on typical self-assembled structures; the formation processes of typical self-assembled structures such as double helices and single helices. See DOI: 10.1039/c2sm25397f

and attractive regions, respectively. The attractive region may refer to the patch with hydrophobicity or hydrogen bonds on the Janus particle surface, and the Janus balance is employed to describe the size of the attractive patch. Intriguingly enough, besides micelles, wormlike strings, and bilayers, we observe several striking types of aggregated structures, which can be attributed to the deformability and anisotropic features of soft Janus particles.

2 Model and simulation details

We describe the deformable and non-centrosymmetric character of soft Janus particles *via* a soft and anisotropic attractive potential, inspired by the soft-particle model in dissipative particle dynamics (DPD)[32] and the one-patch Kern–Frenkel model.[33] For simplicity, we use the interaction cutoff radius (r_c) as the unit of length, k_BT as the unit of energy, and choose the moment of inertia (I) and the mass (m) of the particle as the units, thus the time unit $\tau = \sqrt{mr_c^2/k_BT}$. The variables and parameters in the following will be given in reduced units. The proposed anisotropic potential is expressed as

$$U_{ij} = \frac{\alpha_{ij}^R}{2}\left(1 - r_{ij}\right)^2 - f^{\nu}\frac{\alpha_{ij}^A}{2}\left(r_{ij} - r_{ij}^2\right), \quad (1)$$

where

$$f = \begin{cases} \cos\dfrac{\pi\theta_i}{2\beta}\cos\dfrac{\pi\theta_j}{2\beta} & \text{if } \cos\theta_i \geq \cos\beta \text{ and } \cos\theta_j \geq \cos\beta \\ 0 & \text{otherwise.} \end{cases}$$

As illustrated in Fig. 1a, the red part of surface represents the attractive patch and the green part represents the repulsive region, and the directions of the attractive patches on particle i and j are specified by unit vectors $\boldsymbol{n}_i$ and $\boldsymbol{n}_j$, respectively. θ_i is the angle between $\boldsymbol{n}_i$ and the interparticle vector $\boldsymbol{r}_{ji} = \boldsymbol{r}_j - \boldsymbol{r}_i$, and θ_j is the angle between $\boldsymbol{n}_j$ and $\boldsymbol{r}_{ij} = -\boldsymbol{r}_{ji}$. The size of the attractive patch is described by the Janus balance β, which is half of the opening angle of the attractive patch, and the fraction of surface covered by the attractive patch χ is related to β by the relation $\chi = \sin^2\left(\frac{\beta}{2}\right)$.[14,33]

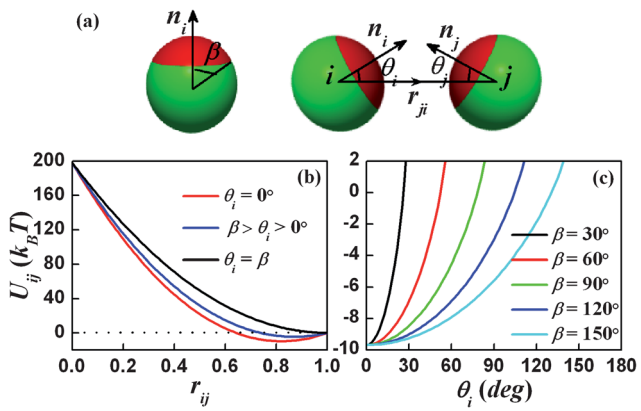

Fig. 1 (a) Model of soft Janus particles. (b) Distance dependence of the anisotropic attractive potential U_{ij} for different θ_i. (c) Angle dependence of U_{ij} with $r_{ij} = 0.8$ for different Janus balance β. In this figure, we choose $\alpha_{ij}^R = 396$, $\alpha_{ij}^A = 220$, $\nu = 1/2$, and $\theta_j = 0°$.

In eqn (1), the magnitude of α_{ij}^R controls the strength of repulsion, α_{ij}^A controls the strength of attraction between the attractive patches, and ν controls the angular width of the attraction. Thus, both α_{ij}^A and ν control the flexibility of the Janus particle aggregates. As shown in Fig. 1b, the distance dependence of U_{ij} presents an explicitly weak attraction at long range while $\theta_i = 0°$, and the strength of the attraction will decrease with increasing θ_i. Therefore, it is clear that the patch-to-patch alignment of soft Janus particles is energetically favorable. The anisotropic function f ensures that the attractive interactions between soft Janus particles are monotonically decreasing from the maximum to 0 and have similar shapes when the Janus balance β ranges from 0° to 180°, as shown in Fig. 1c.

In fact, when $\theta_i = \theta_j = 0°$, eqn (1) becomes an isotropic potential with a shallow attractive well. Thus α_{ij}^R can be related to the linear elastic modulus of the particle, E, by $\alpha_{ij}^R = \pi E d^2/6$,[34,35] where d is the effective diameter of the soft Janus particle. The effective diameter d can be estimated by $d = (\alpha_{ij}^R + \alpha_{ij}^A/2)/(\alpha_{ij}^R + \alpha_{ij}^A)$. If we define δ as the range of attraction relative to the effective diameter d, and $(1 + \delta)d = r_c$, then δ is also related to α_{ij}^R and α_{ij}^A by $\delta = \alpha_{ij}^A/(2\alpha_{ij}^R + \alpha_{ij}^A)$. The energy minimum of the attractive potential at $r_{ij} = d$ gives $G = -U_{ij}^{min} = \alpha_{ij}^A(1 - d)/4$, where the adhesion energy G determines the association strength between particles. Thus we have defined simulation parameters α_{ij}^R and α_{ij}^A from particle properties E, d, and G, and can also estimate the parameter δ. Once E and d, or d and G are known, the simulation parameters α_{ij}^R and α_{ij}^A will be fixed. In reality, the linear elastic modulus E and particle size d can be measured by experiment,[36] and the adhesion energy G, which can also be measured by experiment,[30,37] may be tuned by altering the salt concentration, pH, or temperature.[30,34,37] Therefore, our model can be directly mapped onto a specific experimental system when E and d, or d and G are known. For example, if the model is applied to describe the experimental system in which the diameter of the Janus particles is roughly 20 nm (*i.e.* the reduced unit of length r_c in the model approximately corresponds to 20 nm), the simulation parameters α_{ij}^R and α_{ij}^A will be fixed from the experimentally measurable properties E, d, and G given in the first three columns in Table 1. As shown in Table 1, the simulation parameter α_{ij}^R will increase with the increase of E, and δ will increase with the decrease of E due to the deformability of soft Janus particles. Therefore, our model can successfully reflect the physical nature of soft Janus particles between near-hard-sphere and ultra-soft colloidal systems, and can also be directly mapped onto experimental systems with different ambient conditions.

Table 1 The corresponding relation between the simulation parameters α_{ij}^R and α_{ij}^A and the experimentally measurable properties E, d, and G. The parameters α_{ij}^R, α_{ij}^A, and δ are given in reduced units

E [Pa]	d [nm]	G [k_BT]	α_{ij}^R	α_{ij}^A	δ
9.20×10^5	16.00	2.00	60	40	0.25
1.30×10^6	16.60	2.00	96	48	0.20
2.08×10^6	17.40	2.00	174	61	0.15
4.14×10^6	18.20	2.00	396	88	0.10
1.45×10^7	19.00	2.00	1596	168	0.05
3.23×10^8	19.80	2.00	39 996	808	0.01

We perform NVT simulations of a system of 2.4×10^4 particles in a $20 \times 20 \times 20$ cubic box with periodic boundary conditions. The weak coupling Berendsen thermostat is used to control the temperature at target value.[38] The number of Janus particles is $N_{\text{solute}} = 24\,000 \times \phi$, and the number of spherical solvent particles is $N_{\text{solvent}} = 24\,000 \times (1 - \phi)$ (ϕ is the concentration of Janus solute particles). The solute–solvent and solvent–solvent interactions follow the first term of eqn (1). A time step $\delta t = 0.002\tau$ is used. It should be noted that the coarse-grained model may lead to the reduction in the degrees of freedom of the solvent particles, and therefore, result in different entropy. But this problem may be partially solved by constructing an effective coarse-grained potential which is designed to reproduce correct structure and thermodynamic properties of a given system at a specific condition.[32,34,35,39,40]

3 Results and discussion

In the simulations, we choose $\alpha_{11}^R = \alpha_{22}^R = 396$ (1: Janus particle; 2: solvent particle), $\phi = 5\%$, and $\nu = 1/2$ as in ref. 13. As shown in Table 1, the corresponding elastic modulus E of the Janus particles is approximately equal to 4.0 MPa. Thus, the choice of α_{11}^R ensures that the Janus particles in our simulations are soft and compressible as compared to the usual hard-sphere particles with a modulus of about 2.0 GPa.[34] Changing the repulsion strength α_{12}^R between the Janus and solvent particles corresponds to varying the solvent conditions. For simplicity, we keep athermal solvent conditions with $\alpha_{12}^R = 396$. Each of the simulations starts from an initially isotropic configuration.

Upon varying the Janus balance β and the strength of attraction α_{11}^A (*i.e.* the adhesion energy G), the phase diagram of the soft Janus particles is obtained from a series of simulations, as shown in Fig. 2a. Typical equilibrium self-assembled structures marked by star symbols in Fig. 2a are also presented in Fig. 2. We check the equilibration of our simulations by the snapshots of the systems at different time steps and the time evolution of the distribution $N(s)$ of the number of contacts per Janus particle s (introduced in the following). We have also simulated the systems from different initial configurations to verify the equilibrium structures. As shown in Fig. 2a, all self-assembled structures may be classified into four main regions: micelles (Region A), strings (Region B), bilayers (Region C), and complex supermicelles (Region D). While $\beta \leq 105°$, *i.e.* the fraction of the surface covered by the attractive patch $\chi \leq 0.63$, the micellar clusters (Fig. 2b) with narrow size distribution are obtained (*cf.* Region A in Fig. 2a). The cluster sizes can be controlled by tuning β and α_{ij}^A. With increasing β, as shown in Region B1 of Fig. 2a, Janus particles can self-assemble into wormlike strings (Fig. 2c). Surprisingly, double helices (Fig. 2d) and single helices (Fig. 2e) can be observed at larger β and/or α_{ij}^A, as indicated by Regions B2 and B3 of Fig. 2a. These helical structures are very similar to the helical ribbons observed in experiments.[25] With further increasing β and/or α_{ij}^A, we obtain bilayers (Fig. 2f) and even tetragonal bilayers (Fig. 2g) with two non-close-packed square lattice surfaces as presented in Regions C1 and C3 of Fig. 2a. Meanwhile, we observe the coexisting phases of vesicles and bilayers or tetragonal bilayers in Region C2 of Fig. 2a, whose structures are shown in Fig. 2h and i. When α_{11}^A is small or $\beta \geq 145°$ (Region D of Fig. 2a), the characteristic

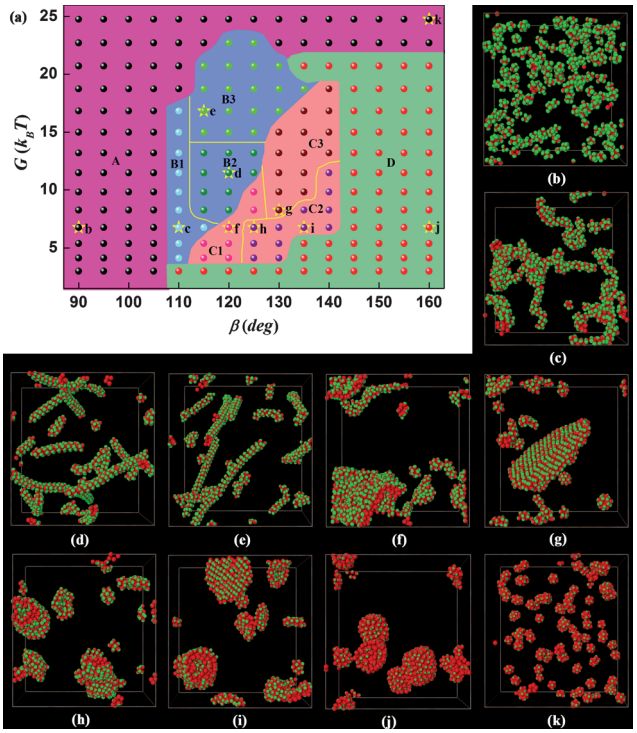

Fig. 2 (a) Phase diagram of soft Janus particles in the G–β plane. Symbols refer to the simulation results, phase boundaries are drawn schematically to guide the eye. Typical equilibrium self-assembled structures marked by star symbols are also shown: (b) micelles; (c) wormlike strings; (d) double helices; (e) single helices; (f) bilayers; (g) tetragonal bilayers; (h) and (i) coexisting phases of vesicles and bilayers or tetragonal bilayers; (j) complex supermicelles with cores comprised of several Janus particles; (k) micelles. For the sake of clarity, we only show Janus solute particles in these systems.

of the anisotropic attraction of the Janus particles is weakened and the aggregation behavior is quite similar to that of isotropic attractive particles. Then soft Janus particles aggregate into large complex supermicelles with the cores being comprised of several Janus particles (Fig. 2j). When α_{11}^A is large enough, the micellar clusters without cores (as shown in Fig. 2k) can be observed again, and the corresponding phase region resides in the top-right corner of Region A in Fig. 2a. The finite size effect is negligible in our simulations (Fig. S1†). The novel tetragonal bilayer and helical structures may have great potential in nanotechnology and biotechnology.

Moreover, we investigate the effect of particle concentration ϕ on typical equilibrium self-assembly structures marked by star symbols b–k in Fig. 2a. These self-assembled structures at different particle concentrations are presented in the ESI†, Fig. S2–S11. We find that the particle concentration has no noticeable effect on micellar clusters, wormlike strings, double helices, and single helices, which are all stable in the concentration range of 1% to 20%. For the state points marked by star symbols f–i in Fig. 2a, when $\phi \leq 1\%$, we can only observe micellar clusters due to the finite particle numbers. The bilayers and tetragonal bilayers are verified up to the higher particle concentration $\phi = 20\%$, as shown in Fig. S6 and S7†. But the coexisting phases of vesicles and bilayers or tetragonal bilayers are easier to turn into tetragonal bilayers at higher particle

concentration (Fig. S8 and S9†). With the increase of particle concentration, the size of complex supermicelles becomes larger because of the aggregation behavior similar to that of isotropic attractive particles. For the state point marked by star symbol k in Fig. 2a, at higher particle concentration ($\phi = 20\%$), the micellar clusters may interconnect between each other and form wormlike micelles (Fig. S11†). Therefore, in relatively dilute solutions (with an approximate particle concentration range of 3% to 10%), the particle concentration ϕ has no noticeable effect on the self-assembled structures and the phase diagram in the G–β plane presented in Fig. 2.

The strength of attraction α_{11}^{A} (or G) and the Janus balance β coordinate to generate a number of fascinating superstructures as shown in Fig. 2. Increasing α_{11}^{A} and β has similar influences on the self-assembled structures, but with different physical nature. Increasing β represents larger patch size and allows larger assemblies. In essence, increasing α_{11}^{A} corresponds to broadening the range of attraction δ (Table S1†). At small α_{11}^{A}, δ is short as compared to particle size, and particle clustering favors densely packed structures with at most six nearest neighbors.[18] At relatively larger α_{11}^{A}, δ becomes larger, which results in a higher deformability of the soft Janus particles, then open and ordered structures are allowed to form and the number of nearest neighbors will exceed six.

In order to fully understand the effects of α_{11}^{A} and β on self-assembled structures, we monitor the distribution $N(s)$ of the number of contacts between the attractive patches per Janus particle, s, as shown in Fig. 3a. $N(s) = N_p(s)/(sN_{solute})$, where $N_p(s)$ is the number of Janus particles with the number of contacts s, N_{solute} is the total number of Janus particles in the system, and $\sum_s N_p(s) = N_{solute}$. Thus, the distributions $N(s)$ in Fig. 3a have been normalized so that $\sum_s sN(s) = 1$. The number of contacts per Janus particle s is calculated including the central Janus particle itself so that s can also represent the cluster size of the micellar structures in Region A of Fig. 2a (here, $N(s)$ can also represent the cluster size distribution), thus the number of nearest neighbors per Janus particle equals $s - 1$. At small α_{11}^{A} and/or β, we can obtain micelles with narrow size distribution, and the size ranges from $s = 2$ to 7. At larger α_{11}^{A} and/or β, *i.e.* for the self-assembled structures shown in Fig. 2b–g, the number of nearest neighbors per Janus particle gradually increases without being limited to six nearest neighbors, as shown in Fig. 3a. However, it cannot exceed seventeen because of the anisotropy of soft Janus particles. These self-assembled structures with more nearest neighbors are energetically favorable, since more contacts are formed between the attractive patches. Thus, the striking self-assembled structures, such as double helices and single helices, are all obtained from the fusion of relatively unstable micellar clusters with fewer nearest neighbors, as demonstrated by the dynamic process shown in the ESI†, Fig. S12–S14.

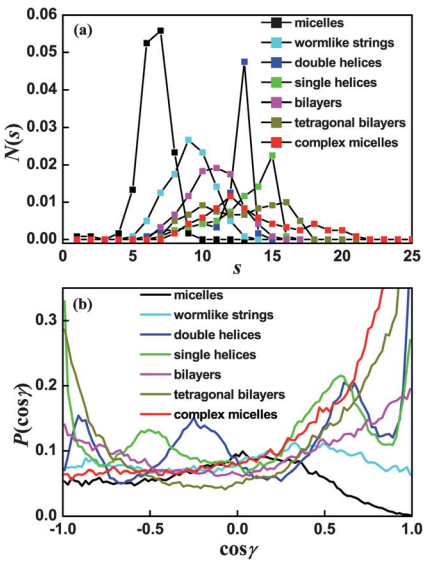

Fig. 3 Relative distributions of neighboring particles in typical self-assembled structures shown in Fig. 2. (a) Distribution $N(s)$ of the number of contacts between the attractive patches per Janus particle s. The distributions have been normalized so that $\sum_s sN(s) = 1$. (b) Distribution of the scalar product between the unit vectors of all pairs of contacted Janus particles ($\cos\gamma = \boldsymbol{n}_i \cdot \boldsymbol{n}_j$).

To provide evidence of different ordered superstructures in our simulations, we calculate the distribution of $\cos\gamma = \boldsymbol{n}_i \cdot \boldsymbol{n}_j$ for all pairs of contacting Janus particles, as shown in Fig. 3b. The distribution $P(\cos\gamma)$ is expected to show well-defined peaks for an ordered state and to be flat in a completely disordered state.[14,15] The face-to-face (antiparallel patches), perpendicular patches, and side-by-side (parallel patches) alignments of Janus particles are characterized by the peaks at $\cos\gamma = -1.0$, 0, and 1.0, respectively. For the micelles with high surface curvature, there is a large probability for closely perpendicular patch alignment ($\gamma \approx 90°$), so the distribution shows a peak at $\cos\gamma \approx 0$. For the wormlike strings, all alignments are possible, and the distribution is quite flat. As can be seen in Fig. 3b, $P(\cos\gamma)$ shows a clear double-peaked shape at $\cos\gamma = -1.0$ and $\cos\gamma = 1.0$ for bilayers, and it is more apparent for tetragonal bilayers due to its planar bilayer structure. Besides the double-peaks at $\cos\gamma \approx -1.0$ and $\cos\gamma \approx 1.0$, double helices and single helices also show two additional peaks between $\cos\gamma = -1.0$ and $\cos\gamma = 1.0$, but the positions of these additional peaks are different. For single helices, Janus particles in the same layer perpendicular to the helix axis pack more closely to a regular hexagon, thus the peak at $\cos\gamma \approx 0.5$ is shown by nonparallel nearest neighbors, and the peak at $\cos\gamma \approx -0.5$ arises from nonparallel next-nearest neighbors. For double helices, the regular hexagon is largely stretched to increase the pitch of helices, so the former three peaks move together toward larger values of $\cos\gamma$. For large complex supermicelles with small surface curvature, the side-by-side alignment of Janus particles is dominating, thus a very strong peak at $\cos\gamma \approx 1.0$ is observed, as shown in Fig. 3b.

4 Conclusions

In conclusion, we propose a mesoscale model which is suitable to describe the deformable and non-centrosymmetirc characteristics of soft Janus particles. The self-assembly of soft Janus particles in dilute solutions is successfully investigated with the aid of the simulation model. The strength of attraction α_{11}^{A} and Janus balance β coordinate to generate a number of fascinating superstructures. We further describe the phase diagram of soft Janus particles with Janus balance *versus* the strength of attraction. It is clear that soft Janus particles provide a rich

palette for the design of novel and exciting hierarchical superstructures. It is expected that chemists and engineers will prepare well-defined soft Janus particles, provide experimental verifications for the phase diagram, and look into the possible applications. These soft anisotropic building blocks may bring new excitement to nanotechnology and biotechnology. Our mesoscale simulation strategy represents a useful route to study the self-assembly of soft anisotropic particles and provides insight into the design and fabrication of novel and complex self-assembled superstructures.

Acknowledgements

This work is subsidized by the National Basic Research Program of China (973 Program, 2012CB821500). The authors also appreciate the financial support from the National Science Foundation of China (21104084, 21074137, 21025416). Z.W.L. acknowledges the support of the China Postdoctoral Science Foundation (20100480069, 201104531) and the K. C. Wong Education Foundation.

References

1 S. C. Glotzer, *Science*, 2004, **306**, 419.
2 S. C. Glotzer and M. J. Solomon, *Nat. Mater.*, 2007, **6**, 557.
3 K.-H. Roh, D. C. Martin and J. Lahann, *Nat. Mater.*, 2005, **4**, 759.
4 A. Walther and A. H. E. Müller, *Soft Matter*, 2008, **4**, 663.
5 F. Wurm and A. F. M. Kilbinger, *Angew. Chem., Int. Ed.*, 2009, **48**, 8412.
6 J. Du and R. K. O'Reilly, *Chem. Soc. Rev.*, 2011, **40**, 2402.
7 S. Jiang, Q. Chen, M. Tripathy, E. Luijten, K. S. Schweizer and S. Granick, *Adv. Mater.*, 2010, **22**, 1060.
8 M. D. McConnell, M. J. Kraeutler, S. Yang and R. J. Composto, *Nano Lett.*, 2010, **10**, 603.
9 A. B. Pawar and I. Kretzschmar, *Macromol. Rapid Commun.*, 2010, **31**, 150.
10 Z. Nie, W. Li, M. Seo, S. Xu and E. Kumacheva, *J. Am. Chem. Soc.*, 2006, **128**, 9408.
11 M. Lattuada and T. A. Hatton, *J. Am. Chem. Soc.*, 2007, **129**, 12878.
12 R. Fantoni, A. Giacometti, F. Sciortino and G. Pastore, *Soft Matter*, 2011, **7**, 2419.
13 L. Hong, A. Cacciuto, E. Luijten and S. Granick, *Langmuir*, 2008, **24**, 621.
14 F. Sciortino, A. Giacometti and G. Pastore, *Phys. Chem. Chem. Phys.*, 2010, **12**, 11869.
15 F. Sciortino, A. Giacometti and G. Pastore, *Phys. Rev. Lett.*, 2009, **103**, 237801.
16 W. L. Miller and A. Cacciuto, *Phys. Rev. E: Stat., Nonlinear, Soft Matter Phys.*, 2009, **80**, 021404.
17 Y. Ding and M. Kröger, *Macromolecules*, 2009, **42**, 576.
18 Q. Chen, J. K. Whitmer, S. Jiang, S. C. Bae, E. Luijten and S. Granick, *Science*, 2011, **331**, 199.
19 Q. Chen, S. C. Bae and S. Granick, *Nature*, 2011, **469**, 381.
20 F. Romano and F. Sciortino, *Nat. Mater.*, 2011, **10**, 171.
21 F. Romano and F. Sciortino, *Soft Matter*, 2011, **7**, 5799.
22 R. Erhardt, A. Böker, H. Zettl, H. Kaya, W. Pyckhout-Hintzen, G. Krausch, V. Abetz and A. H. E. Müller, *Macromolecules*, 2001, **34**, 1069.
23 R. Erhardt, M. Zhang, A. Böker, H. Zettl, C. Abetz, P. Frederik, G. Krausch, V. Abetz and A. H. E. Müller, *J. Am. Chem. Soc.*, 2003, **125**, 3260.
24 M. Bradley and J. Rowe, *Soft Matter*, 2009, **5**, 3114.
25 V. Percec, D. A. Wilson, P. Leowanawat, C. J. Wilson, A. D. Hughes, M. S. Kaucher, D. A. Hammer, D. H. Levine, A. J. Kim, F. S. Bates, K. P. Davis, T. P. Lodge, M. L. Klein, R. H. DeVane, E. Aqad, B. M. Rosen, A. O. Argintaru, M. J. Sienkowska, K. Rissanen, S. Nummelin and J. Ropponen, *Science*, 2010, **328**, 1009.
26 M. Peterca, V. Percec, P. Leowanawat and A. Bertin, *J. Am. Chem. Soc.*, 2011, **133**, 20507.
27 C. Park, J. Lee and C. Kim, *Chem. Commun.*, 2011, **47**, 12042.
28 C. N. Likos, *Soft Matter*, 2006, **2**, 478.
29 C. A. Angell and K. Ueno, *Nature*, 2009, **462**, 45.
30 D. M. Heyes and A. C. Brańka, *Soft Matter*, 2009, **5**, 2681.
31 M. L. Klein and W. Shinoda, *Science*, 2008, **321**, 798.
32 R. D. Groot and P. B. Warren, *J. Chem. Phys.*, 1997, **107**, 4423.
33 N. Kern and D. Frenkel, *J. Chem. Phys.*, 2003, **118**, 9882.
34 R. D. Groot and S. D. Stoyanov, *Phys. Rev. E: Stat., Nonlinear, Soft Matter Phys.*, 2008, **78**, 051403.
35 R. D. Groot and S. D. Stoyanov, *Soft Matter*, 2010, **6**, 1682.
36 J. Mattsson, H. M. Wyss, A. Fernandez-Nieves, K. Miyazaki, Z. Hu, D. R. Reichman and D. A. Weitz, *Nature*, 2009, **462**, 83.
37 J. K. Cho, Z. Meng, L. A. Lyon and V. Breedveld, *Soft Matter*, 2009, **5**, 3599.
38 H. J. C. Berendsen, J. P. M. Postma, W. F. van Gunsteren, A. DiNola and J. R. Haak, *J. Chem. Phys.*, 1984, **81**, 3684.
39 H. S. Ashbaugh, H. A. Patel, S. K. Kumar and S. Garde, *J. Chem. Phys.*, 2005, **122**, 104908.
40 S. Jain, S. Garde and S. K. Kumar, *Ind. Eng. Chem. Res.*, 2006, **45**, 5614.

Addition and correction

Note from RSC Publishing

This article was originally published with incorrect page numbers. This is the corrected, final version.

The Royal Society of Chemistry apologises for these errors and any consequent inconvenience to authors and readers.